HHS Public Access

Author manuscript

Dev Cell. Author manuscript; available in PMC 2019 March 12.

Published in final edited form as:

Dev Cell. 2018 March 12; 44(5): 624–633.e4. doi:10.1016/j.devcel.2018.01.024.

Enteroid monolayers reveal an autonomous WNT and BMP circuit controlling intestinal epithelial growth and organization

Curtis A. Thorne[1,3,4], **Ina W. Chen**[2,4], **Laura E. Sanman**[2], **Melanie H. Cobb**[1], **Lani F. Wu**[2,*], and **Steven J. Altschuler**[2,*]

[1]Green Center for Systems Biology, Simmons Cancer Center, Department of Pharmacology, University of Texas Southwestern Medical Center, Dallas, TX 75390, USA

[2]Department of Pharmaceutical Chemistry, University of California, San Francisco, San Francisco, CA 94158, USA

[3]Department of Cellular and Molecular Medicine, University of Arizona Cancer Center, University of Arizona, Tucson, AZ 85724, USA

Summary

The intestinal epithelium maintains a remarkable balance between proliferation and differentiation despite rapid cellular turnover. A central challenge is to elucidate mechanisms required for robust control of tissue renewal. Opposing WNT and BMP signaling is essential in establishing epithelial homeostasis. However, it has been difficult to disentangle contributions from multiple sources of morphogen signals in the tissue. Here, to dissect epithelial-autonomous morphogenic signaling circuits, we developed an enteroid monolayer culture system that recapitulates four key properties of the intestinal epithelium, namely the ability to: maintain proliferative and differentiated zones, self-renew, polarize, and generate major intestinal cell types. We systematically perturb intrinsic and extrinsic sources of WNT and BMP signals to reveal a core morphogenic circuit that controls proliferation, tissue organization, and cell fate. Our work demonstrates the ability of intestinal epithelium, even in the absence of 3D tissue architecture, to control its own growth and organization through morphogen-mediated feedback.

eTOC

Thorne, Chen et al. develop an enteroid monolayer culture system that recapitulates cell-type composition, crypt organization, and turnover kinetics of the intestinal epithelium. The authors use the enteroid monolayer to uncover an epithelium-intrinsic Wnt and BMP morphogenic circuit that regulates proliferation and tissue organization in the intestinal epithelium.

*Correspondence to: lani.wu@ucsf.edu and steven.altschuler@ucsf.edu.

[4]These authors contributed equally

Lead contact: steven.altschuler@ucsf.edu

Author Contribution

Conceptualization, C.A.T., L.F.W., S.J.A.; Methodology, Formal Analysis and Investigation, C.A.T., I.W.C., and L.E.S.; Writing, C.A.T., I.W.C., L.E.S., L.F.W., and S.J.A.; Funding Acquisition and Resources, C.A.T., M.H.C., L.F.W., S.J.A.

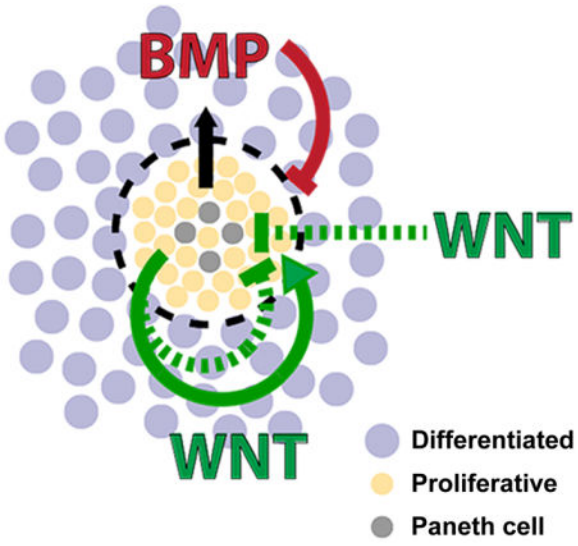

Introduction

The intestinal epithelium has the remarkable ability to maintain crypts that are highly repetitive and uniform in size despite cellular turnover that renews the tissue every four to five days (Crosnier et al., 2006; Radtke and Clevers, 2005). Disruption of crypt homeostasis is a critical event in the progression of intestinal diseases, including inflammatory bowel disease and cancers of the gastrointestinal tract (Maloy and Powrie, 2011; Radtke and Clevers, 2005; Terzić et al., 2010). A central challenge has been to elucidate mechanisms that regulate crypt proliferation and differentiation.

Two opposing factors regulating proliferation in the intestinal epithelium are: WNT, which promotes stem cell renewal, and BMP, which promotes cell differentiation (Auclair et al., 2007; Batts et al., 2006; Fevr et al., 2007; Haramis et al., 2004; He et al., 2004; Qi et al., 2017). WNT and BMP arise from multiple sources in the intestinal tissue (Crosnier et al., 2006). Myofibroblasts in the mesenchyme secrete WNT and BMP, while Paneth cells in the epithelial crypt bases secrete WNT (Batts et al., 2006; Farin et al., 2016; San Roman et al., 2014; Sato et al., 2010). It has also been suggested that differentiated epithelial cells secrete BMP (Batts et al., 2006). Given the redundant sources of signaling, it is unclear what unique role, if any, each source plays in regulating the epithelium. For example, while the formation of intestinal organoids is critically dependent on Paneth cells as a source of WNT signaling, the presence of Paneth cells is dispensable in vivo (Durand et al., 2012; Sato et al., 2010). Understanding how the intestinal epithelium integrates multiple sources of signals requires experimental systems in which different sources of signals can be separated and probed.

The development of 3D organoids provided a critical demonstration that intestinal epithelium has the ability to recapitulate the proliferative crypt-like structures in vitro, even in the absence of mesenchymal tissues (Ootani et al., 2009; Sato et al., 2009, 2011). However, the 3D geometry of the intestinal crypt and villus structures adds yet another layer of complexity, as tissue curvature has the potential to reshape morphogen gradients (Shyer et

al., 2015). Thus with existing culture systems, it is difficult to disentangle the contribution of different morphogen sources and tissue architecture to tissue homeostasis.

Here, we develop an intestinal monolayer culture system that is amenable to high-throughput perturbation and quantification of epithelial cell and tissue phenotypes. We show that these cultures, absent both mesenchyme and tissue curvature, recapitulate four key properties of the intestinal epithelium, namely the ability to: organize cells into proliferative and differentiated zones, self-renew within several days, polarize into apical and basal surfaces, and generate the major intestinal cell types. We use these cultures, which we refer to as “enteroid monolayers,” to systematically perturb WNT and BMP signaling, and investigate the consequences on cell proliferation and organization. We discover that epithelial sources of WNT and BMP signaling are critical in establishing an epithelial-autonomous feedback circuit that regulates tissue proliferation and organization.

Results

Establishing crypt cultures as enteroid monolayers

To systematically study epithelium-intrinsic morphogenic circuits, we sought to develop a feeder-layer free, monolayer enteroid culture system. Previously, it was shown that purified intestinal crypts can give rise to tissue-like organoid structures when embedded in 3D extracellular matrix (ECM) (Sato et al., 2009). These cultures can be grown for short times in planar geometries (Ettayebi et al., 2016; Moon et al., 2014; VanDussen et al., 2015). However, it is unclear if these monolayer cultures spatially organize, maintain stem cell niches, and recapitulate in vivo tissue turnover.

Here, we establish an in vitro planar culture of the intestinal epithelium that recapitulates tissue spatial organization, cell-type composition, and renewal dynamics. To grow intestinal crypts as planar cultures, we first harvested crypts from mouse jejunum using isolation protocols previously published for 3D intestinal organoids (Sato et al., 2009; Whitehead et al., 1987) (Figure S1A and Methods). The isolated crypts were seeded on top of ECM-coated surfaces and cultured in ENR (EGF, Noggin, R-spondin-1) supplemented media. We found that Matrigel-coated surfaces best supported crypt survival compared to poly-L-lysine- or collagen-coated surfaces (Figure S1B). We tested modification to the base ENR media and found that crypt survival was dramatically improved by the addition of 10 μM Rho Kinase (ROCK) inhibitor, Y-27632, and 3 μM GSK-3 inhibitor, CHIR99021, at the time of seeding (Figure S1C). After 4–6 hours, cells were washed and placed in ENR media for the remainder of the culture.

Under these culture conditions, seeded crypts grew out as large, contiguous sheets of epithelium with heterogeneity in cell morphology and densities (Figure 1A,B, Figure S1D). Confocal microscopy images showed that the intestinal cultures formed clear monolayers (Figure 1C,D, Supplementary Movie 1). The monolayer polarized with the apical side facing the media and the basal side attached to the Matrigel coating. Actin bundles formed consistently at the apex of cell-to-cell contacts (Figure 1D). These epithelial cultures were also devoid of mesenchymal cells, indicated by a lack of α-smooth muscle actin (α-SMA) staining (Figure S1E). Taken together, we found the crypt cultures form a planar monolayer

that polarizes with the apical side facing the culture media, hereafter referred to as enteroid monolayers.

Enteroid monolayer cultures recapitulate in vivo crypt-like regions and major cell types

We next investigated the spatial properties of the enteroid monolayers. We observed that the epithelial sheets contain distinct dense compartments (Fig 1A, arrowheads). These dense clusters contain proliferative cells (EdU^+) and are surrounded by large areas of non-proliferative cells (Figure 1B,C,E; Figure S1F). The small, tightly packed EdU+ regions also co-stained positively for the proliferation marker Ki67, further confirming that these are putative crypt zones in the culture (Figure 1F, top row).

To investigate the cell-type composition of the enteroid monolayer cultures, we stained for the major cell types of the intestinal epithelium. Cell-fate markers revealed that intestinal stem cells ($Olfm4^+$, $LGR5\text{-}GFP^+$) were present in the center of the proliferative zones while enterocytes ($Villin1^+$ ($Vil1^+$)) made up the surrounding area (Figure 1E, F, Supplementary Movie 2). Other intestinal cell types, including Goblet ($Mucin\text{-}2^+$ ($Muc2^+$)), Tuft ($DCLK\text{-}1^+$), enteroendocrine (chromogranin A^+ ($ChgA^+$)) and Paneth ($UEA\text{-}1^+$, $CD24^+$) cells, were also present in the culture (Figure 1F, Figure S1G). Additionally, we observed that stem cells reside adjacent to Paneth cells, recapitulating their spatial arrangement in vivo (Figure 1E).

We next investigated whether crypt formation and organization in the enteroid monolayers is an intrinsic property of the intestinal epithelium or whether it is due to maintenance of patterns formed in vivo. To investigate this, we enzymatically and mechanically dissociated 3D organoids into single cells and small cell clusters before seeding into planar cultures (Figure S2A). We observed that proliferative crypt-like foci are formed within a few days, indicating the ability of the cultures to self-organize (Figure S2B, C). The proliferative crypt-like foci contained Paneth cells juxtaposed with Lgr5+ stem cells, recapitulating their arrangement in primary enteroid monolayers and in vivo (Figure S2D). As with enteroid monolayer cultures derived from primary intestinal cells, cultures from dissociated 3D organoids were maintained for two weeks and generated mature epithelial cell types including Paneth, stem, Goblet, and enteroendocrine cells (Figure S2E). Quantification of the total cell number, crypt number, percent of proliferative cells (EdU+), and percent of Paneth cells (Lyz+) revealed that the crypt number and proliferative population were still expanding at 14 days of culture (Figure S2F, G, H, I), indicating that the cultures did not reach homeostasis during this time frame Finally, in addition to small intestine cultures, we were able to culture mouse colonic epithelium in 2D with the addition of WNT3a to the culture medium (Figure S3A).

Thus, even when intestinal epithelial cells are constrained to planar surfaces, they are able to maintain proliferative and differentiated compartments, self-organize, and produce the major intestinal cell types. Due to their similarity to in vivo crypts and villi in terms of tissue organization and cell-type composition, we refer to the proliferative and nonproliferative (differentiated) zones as “crypt-like foci” and “villus-like regions”, respectively (Figure S1F). To quantify these cell- and tissue-level properties, we developed image-processing algorithms that identify individual cells as well as crypt regions of the tissue (Figure S3B

and Methods). Taken together, the enteroid monolayer cultures organize into crypt-like and villus-like regions, wherein crypt-like regions contain juxtaposed stem and Paneth cells surrounded by proliferative non-stem cells (TA cells), while villus-like regions contain the remaining differentiated cell types, including enterocyte, Goblet, enteroendocrine, and tuft cells.

Enteroid monolayers recapitulate in vivo renewal kinetics

We then investigated the turnover dynamics of enteroid monolayers. In the first 24 hours post seeding, crypt fragments adhere and spread out in an unorganized fashion (as shown by dispersion of EdU^+ cells) (Figure 2A). Over the next 48 hours, these proliferative regions self-organized into densely packed circular zones surrounded by larger, less compact regions of non-proliferative cells (Figure 2A).

We quantified the tissue renewal rate with a pulse-chase experiment using EdU labeling (Figure 2B, C, D). Immediately after the initial two-hour pulse, EdU^+ cells were observed in compact regions and co-stained with the proliferation marker Ki67. After a 48 hour chase, a subset of the EdU^+ cells began to co-stain with the enterocyte marker villin, indicating differentiation and migration out of the crypts. After a 72–96 hour chase, the EdU signal was largely lost from the culture, indicating labeled cells were shed from the tissue. These results suggest that cells within the enteroid monolayer cultures renew at a 4–5 day rate, which is similar to the kinetics observed in vivo (Cheng and Leblond, 1974). Finally, we tracked cell-type composition over two weeks of culture. We observed an initial burst of tissue expansion in the first three days followed by stabilization of cell number after 1–2 weeks of culture (Figure 2E). Characterization of crypt cells (stem, Paneth, and EdU+ cells) show that these cell types make up a stable fraction of the tissue during the same 2 weeks of culture, indicating that while tissue size may fluctuate, crypt units remained relatively constant over time.

Consistent with the migration of cells away from crypt foci, apoptosis was observed at the margins of the differentiated zones of the enteroid monolayer cultures, comparable to anoikis of cells at villus tips in vivo (Figure 2F, G). In addition, we observed partly-dissociated nuclei above the tissue plane reminiscent of cell extrusion (though it is currently unclear whether these cells are alive or apoptosing at the time of shedding; Figure S3C). Shedding of cells produced cell fragment debris into the media that can be observed within 24 hours after media change.

Taken together, our enteroid monolayer cultures closely mimic in vivo intestinal epithelial tissue in that they: 1) polarize into a monolayer with apical/basolateral surfaces, 2) maintain proliferative crypt-like and differentiated villus-like regions, 3) differentiate into all the major cell lineages, 4) self-organize and 5) undergo renewal kinetics similar to in vivo rates. Thus, the enteroid monolayer culture system recapitulates key features of the intestinal epithelium tissue, and allowed us to investigate epithelial-intrinsic signaling in a planar tissue without mesenchymal contributions.

Extrinsic WNT and BMP signals modulate proliferation and organization in enteroid monolayers

WNT and BMP signals control intestinal epithelium proliferation in vivo and in 3D organoids. Thus, we investigated how modulating WNT and BMP signals alter proliferation in enteroid monolayers, which lack intestinal mesenchymal cells and 3D geometric structure.

To assess how Wnt and BMP signals interact, we made use of the high-throughput capabilities of our enteroid monolayer system. First, we determined the active range of WNT and BMP concentrations, which bracketed EC_{50} values of 1 nM and ~10 nM, respectively (we note that enteroid culture conditions contained 50ng/ml Noggin, an inhibitor of BMP, which simply induced a 10-fold shift of EC50; Figure S3D,E,F). Second, we stimulated enteroid monolayers in microtiter plates with combinations of varying WNT3a and BMP4 concentrations (Methods). Finally, after two or five days of culture, we quantified the effects of the morphogens (Figure 3) on total cell number (Figure 3A,D), crypt number (Figure 3B,E), and crypt size (average number of cells per crypt; Figure 3C,F).

Congruous with in vivo studies, we observed that, after two days, WNT and BMP have opposing effects on proliferation and size of crypt-like regions: increased WNT or decreased BMP led to increased cell numbers and more numerous and enlarged crypt regions (Figure 3A, D). Unexpectedly, we noticed a striking change in the organization of crypt foci as we moved through the WNT/BMP response landscape (Figure 3A). In the control condition, we observed circular and compact crypt foci (Figure 3A, upper right corner). With increased WNT, the proliferative regions greatly expanded and lost circularity (Figure 3A, upper left corner). In contrast, with increased BMP, proliferative regions shrink yet remained compact and circular (Figure 3A, lower right corner). Simultaneously increasing both WNT and BMP caused moderate proliferation but disorganized proliferative zones (Figure 3A, lower left corner). Overall, the response landscape reveals a multi-phasic response to WNT and BMP morphogens and demonstrates that externally supplied WNT disrupted crypt organization.

Intrinsic WNT and BMP signals are critical for tissue organization in enteroid monolayers

Next, we investigated the effects of epithelial sources of WNT and BMP signaling. First, in the epithelium, WNT is primarily derived from the Paneth cells embedded in the crypt base, and is thought to spread through division of proliferative cells (Farin et al., 2016). In the context of the enteroid monolayers, endogenous WNT signaling is likely present and essential as the WNT co-regulator R-spondin 1(RSPO) was required even when no external Wnt was supplied (Figure S4A,B). Second, epithelial sources of BMP mRNA have been reported to arise from differentiated cells (Batts et al., 2006). In the context of the enteroid monolayers, we observed that BMP2 proteins are present in cells in the differentiated villus-like regions (Figure S4C). We further observed that BMP2 protein is absent from the proliferative crypt-like regions, indicating that the differentiated cells are the source of BMP signals in the tissue (Figure S4C). Upon BMP treatment, phosphorylation of the BMP effector SMAD1/5 can be found throughout the epithelium, indicating that all cells in the enteroid tissue responded to BMP signaling (Figure S4D).

To characterize the function of epithelial-derived signaling on tissue homeostasis, we inhibited WNT signaling via IWP-2, a potent and specific Porcupine inhibitor, and inhibited BMP signaling via LDN-193189 (LDN), a BMP type I receptor inhibitor (Chen et al., 2009; Cuny et al., 2008). The effects on tissue growth were monitored up to 72 hours after seeding. After 48 hours, visual inspection of the enteroids showed that LDN treatment caused an increase in proliferation, whereas IWP-2 treatment caused a decrease in proliferation (Figure 4A). Quantification of tissue growth under these perturbations confirmed these trends, showing that epithelial-derived Wnt and BMP functionally regulate tissue proliferation in the enteroid monolayers (Figure 4B,C).

Finally, we investigated the role of epithelial-intrinsic signals in organization of the tissue into crypt-like foci. Blocking epithelium-intrinsic BMP signaling (no extrinsic BMP was supplied to the media) with LDN treatment led to disorganization of the crypt-like regions despite increased proliferation (Figure 4A). When we blocked WNT secretion with IWP-2, proliferative clusters were lost (and thus organization of clusters could not be assessed). To see whether externally supplied WNT can rescue the loss of intrinsic WNT signaling, we co-treated the enteroid monolayers with IWP-2 and WNT3a. Interestingly, this co-treatment rescued the proliferative population of the enteroid monolayers (Figure 4D, Figure S4E). However, the organization of proliferative cells into crypt foci was not restored (Figure 4E). To quantitatively measure the dispersion of proliferative cells, we computed the distance between nearest neighbor pairs of proliferative (EdU+) cells in crypts (Experimental Procedures). In untreated crypts, the proliferative cluster is tightly packed with a robust mean nearest neighbor distance of 11.263±0.161 μm (mean±SD; Figure S4F). Under IWP-2 and WNT3a treatment, the mean nearest neighbor distance significantly increases (p-value = 1.53×10^{-5} as determined by Student's unpaired t-test; Fig 4F), suggesting epithelial-derived sources of WNT are needed for the compact organization of crypt-like foci. Thus, epithelial-intrinsic sources of WNT and BMP play critical functional roles in regulating crypt organization.

Taken together, we have shown that enteroid monolayers, derived from primary intestinal epithelium, maintain their own sources of WNT and BMP, and that these sources are functional in regulating the proliferation of the tissue. Further, the epithelial sources of WNT and BMP work in concert to establish and maintain spatial organization of the tissue into crypt-like foci and villus-like regions.

An autonomous WNT and BMP feedback circuit controls tissue proliferation

Finally, we examined how epithelial sources of WNT and BMP interact to regulate proliferation. While we observed that the addition of WNT increased tissue proliferation for the first 48h of treatment, WNT3a treatment caused a decrease in proliferation and a loss of crypts after 72 hours (Figs. 4A,B). We hypothesized that this decrease could be due to feedback from differentiated cells, via factors that inhibit proliferation. We previously observed that BMP2 proteins are produced by the differentiated cells in the culture and that the number of cells increases under WNT3a stimulation (Figure 3, Figure S4C). The combined effect would be an increase in total BMP2 protein in the culture. Previous studies have shown that BMP signaling inhibits proliferation and stem cell signaling (Auclair et al.,

2007; Qi et al., 2017). Thus, WNT3a treatment could generate an influx of differentiated cells that then produce additional BMP signals, which feeds back to inhibit the WNT-driven proliferation. To test the hypothesis that production of BMP from increasing production of differentiated cells causes the decrease observed in WNT-induced proliferation, we blocked BMP signaling in WNT-treated enteroids using LDN. As predicted, LDN treatment abolished the reversal of proliferation and crypt expansion under long-term WNT3a treatment (Figure 4G). Thus, time-delayed negative feedback from intrinsic BMP signals could serve to counterbalance an increase in WNT signals to maintain a homeostatic ratio of proliferation and differentiation.

Interestingly, Paneth cells both secrete WNT to promote stem cell renewal and require WNT to fully differentiate (van Es et al., 2005; Farin et al., 2016). This presents a putative positive feedback (Farin et al., 2012): WNT drives proliferative cells to differentiate into Paneth cells, which in turn secrete more WNT, leading to expansion of stem cells, proliferative cells and Paneth cells. However, unchecked proliferation of Paneth cells is not observed in healthy tissues, indicating mechanisms exist to regulate their numbers (Clevers and Bevins, 2013; Sato et al., 2010; Snippert et al., 2010). To explore the regulation of Paneth cell number, we examined the response of enteroid monolayers to a range of WNT3a and BMP4 concentrations at 48 hours (Figure 4H). We found that concentrations ≥1 nM WNT decreased the fraction of Paneth cells by 47.36% (Figure 4H, rows). BMP, on the other hand, had no observable effect (Figure 4H, columns). The WNT-induced decrease in Paneth cell fraction was due to overall expansion of the tissue as well as loss in absolute numbers of the Paneth cells (Figure S4G, H). These results suggest that intestinal epithelium may have the ability to respond to elevated WNT concentrations by down-regulating the source of epithelial WNT, the Paneth cell.

Discussion

Previous studies have established the critical importance of opposing WNT and BMP signaling in controlling homeostasis of the intestinal epithelium (Fevr et al., 2007; Haramis et al., 2004; He et al., 2004; San Roman et al., 2014). However, there are multiple tissue sources that can provide WNT and BMP to the intestinal epithelium. It is therefore challenging to disentangle the contribution of each of these sources to epithelial homeostasis in vivo. Using an enteroid monolayer culture system, we evaluated the contributions of epithelial-intrinsic and extrinsic WNT and BMP to epithelial homeostasis. Our results reveal that epithelial-derived WNT and BMP play a critical role in maintaining tissue proliferation and organization. Interestingly, we observed that while exogenously supplied WNT or BMP have similar effects on proliferation as epithelial-intrinsic WNT or BMP, they cannot rescue lost tissue organization. In addition, we found that enteroid monolayer cultures derived from the colon do not exhibit tight clustering of the crypt regions. This may be due to the exogenously supplied WNT3a that is necessary for culturing colon enteroids or the lack of Paneth cells in colon crypts, which serve as a source of epithelial-intrinsic WNT. Finally, we discovered an autonomous feedback circuit in enteroid monolayers regulating tissue proliferation whereby excessive proliferation driven by WNT is countered by production of differentiated cells that produce BMP. The feedback circuit may also regulate tissue proliferation through down-regulation of the Paneth cell population under high WNT

conditions. Interestingly, it has been shown that up-regulation of WNT signaling through R-spondin stimulation or GSK3 inhibition upregulates Paneth cell numbers, yet this previous study did not use WNT ligands directly (Farin et al., 2012). Thus, the response of Paneth cells to different WNT ligands requires further mechanistic investigation. Taken together, these results demonstrate that the epithelium is capable of regulating its own proliferation and organization through an intrinsic feedback circuit and, more broadly, show that the source of morphogenic signals has a pronounced effect on how these signals regulate tissue proliferation and organization.

Tissue organoid models have become increasingly powerful platforms for understanding tissue organization, modeling disease and identifying novel therapeutics (Boj et al., 2015; Gao et al., 2014; Lancaster et al., 2013; McCracken et al., 2014; Ootani et al., 2009; Warmflash et al., 2014; van de Wetering et al., 2015). In particular, 3D intestinal organoids have been instrumental in interrogating stem cell biology. Recent efforts have led to the development of 2D cultures of differentiated intestinal tissues in transwell format (Ettayebi et al., 2016; Moon et al., 2014; VanDussen et al., 2015). Though these culture systems are important advances, it is unclear whether they self-organize, maintain stem cell niches, or undergo self-renewal.

Our enteroid monolayer cultures have three crucial characteristics. First, they polarize with apical surfaces exposed--in contrast to 3D organoids--which allows facile introduction of luminal contents in a physiologically relevant manner without the need for labor intensive microinjection. Second, they recapitulate key properties of in vivo intestinal epithelium, particularly crypt organization, which has been lacking in previous systems. Third, they can be cultured in microtiter plate format, making them amenable to high-throughput imaging assays and automated quantification of both cell- and tissue-level properties. A limitation of our (and other) organoid systems is that other factors undoubtedly modulate the behaviors of the epithelium in vivo. It remains to be seen how these additional sources of signals are integrated. A further limitation of our system is that cultures currently cannot be easily expanded through resuspension and passaging like classical cell lines. Nevertheless, the enteroid monolayer system described here provides a powerful platform for studying the intestinal epithelium in isolation, that may aid in the identification of regulators of epithelial homeostasis or new therapeutics for intestinal diseases.

Star Methods

Contact for Reagent and Resource Sharing

Further information and requests for resources and reagents should be directed to and will be fulfilled by the Lead Contact, Steven Altschuler (steven.altschuler@ucsf.edu).

Experimental Model And Subject Details

Animals—All animal care and experimentation was conducted under protocols agreed upon by the Administrative Panel on Laboratory Animal Care at the University of California, San Francisco and the University of Texas Southwestern. Mice used in these studies are from C57BL/6 strain (most experiments) or, when indicated, a mutant

Lgr5$^{eGFP\text{-}DTR}$ strain (kind gift of Frederic de Sauvage, Genentech) or a mutant Lgr5$^{EGFP\text{-}IRES\text{-}creERT2}$ strain (kind gift of Hasan Zaki, UTSW). Both female and male mice were used in the study.

Cell Lines—Human BJ fibroblast cells (ATCC #CRL-2522) were cultured on polystyrene plates at 37° C and 5% CO2 and maintained in DMEM media with 10% FBS and antibiotics (penicillin and streptomycin).

Method Details

Crypt isolation and enteroid culture—Murine jejunums were removed from freshly sacrificed 4–16 week old mouse, cut open longitudinally, and washed with cold PBS. The tissues were placed in cold PBS with antibiotics (penicillin and streptomycin), 1.5 mM DTT, 2 mM EDTA, fresh 10 uM Y-27632 and incubated on ice for 30 minutes. Intestines were then moved to a tube with cold PBS with 2 mM EDTA and shaken vigorously for one minute to release crypts into solution. The shaking step was repeated until optimal crypt release is observed. The intestine was then discarded and solution containing crypts were centrifuged at 300 × g for 3 minutes to pellet the crypts. The crypt pellet was then re-suspended in 10ml DMEM with 10% FBS. This wash was repeated two more times and was essential to perform quickly to remove residual EDTA and restore Ca^{++} to the crypts. The crypt suspension was then filtered through a 100 μm strainer followed by a 70 μm strainer to remove large villi fragments. The crypts were pelleted at 150 × g for 3 minutes and re-suspended in 2D attachment media. 2D attachment media consisted of EGF (50 ng/ml, Invitrogen #PMG8043), LDN-193189 (100 nM, Sigma-Aldrich #P4543), R-spondin 1 (1 μg/ml, R&D Biosystems #3474-RS-050), CHIR99021 (10 μM, Selleck #S1263), Y-27632 (10 μM, Selleck #S1049) in basal organoid media. The basal organoid media consists of advanced DMEM/F12 media supplemented with 1x N-2 supplement (Invitrogen #17502-048), 1x B-27 supplement (Invitrogen #17504-044), 10mM HEPES (Invitrogen #15630-080), 1x Glutamax (Invitrogen #35050-061), 1mM N-acetyl-cysteine (Sigma-Aldrich #A9165), 1x penicillin, and 1x streptomycin). The crypts concentration is then estimated using a hemocytometer.

For 2D crypt seeding in 96-well plates, 96-well plates were first coated with growth factor reduced Matrigel (Corning #356231). All experiments were performed in 96 well, Black/Clear, Tissue culture treated plates (Falcon #353219). To coat, 96-well plates were incubated with 50μl of 0.8 mg/ml Matrigel diluted in basal organoid media at 37°C for one hour, which allows Matrigel to polymerize and coat the bottom of the well. From the step above, 50–100 crypts were then seeded into each well of the 96-well plate and incubated in the attachment media for 4 hours. The cells were then washed with media to remove non-adherent villi fragments and placed in supplemented (ENR) organoid media for the remainder of the culture. Supplemented organoid media is basal organoid media supplemented with EGF (50 ng/ml), Noggin (50 ng/ml), and R-spondin (1 μg/ml). For two week time course data, enteroid monolayers were grown in basal media supplemented with 10% R-spondin conditioned media.

Enteroid monolayer seeding from dissociated 3D organoids—For self-organization experiments shown in Figure S2, 3D organoids (grown in supplemented (ENR) organoid media) were sheared into crypt-like structures with a fire-polished Pasteur pipette and then enzymatically digested into single cells and small cell clusters using TrypLE Express (Thermo Fisher #12605010). Cells were washed once with organoid basal media and then resuspended in organoid basal media containing EGF (50 ng/mL), Noggin (50 ng/mL), R-spondin (1 μg/ml), CHIR-99021 (3 μM), and Y-27632 (10 μM). Approximately 50,000 cells were seeded in each well of Matrigel (1:20)-coated 96-well plates. After 24hrs of culture, cells were washed once with organoid basal media and then cultured in supplemented (ENR) organoid media for the remainder of the experiment. For the 2 week time-course experiment, recombinant R-spondin-1 was replaced with 10% R-spondin conditioned media.

Growth factors and small molecules—The concentrations response curves in Figure 3A–C in descending order are as follows: WNT3a (nM) – 4, 2, 1, 0.5, 0.25, 0.125, 0.06, 0.03, 0; BMP4 (nM) – 18, 9, 4.5, 2.25, 1.125, 0.56, 0. The concentrations response curves in Figure 3D–F in descending order are as follows: WNT3a (nM) – 16, 8, 4, 2, 1, 0.5, 0.25, 0.125, 0.06, 0.03, 0; BMP4 (nM) – 36, 18, 9, 4.5, 2.25, 1.125, 0.56, 0. For Figure 4H the concentrations are WNT3a (nM) – 4, 2, 1, 0.5, 0.25, 0.125, 0.06, 0.03, 0; BMP4 (nM) – 9, 4.5, 2.25, 1.125, 0.56, 0.

Staining and click chemistry—All antibody solutions were made in PBS (Life Technologies Gibco #70013). All wash steps were performed three times using 0.1% Tween20 (Fisher Scientific #BP337) in PBS. Antibodies were diluted into 2.5% BSA (Jackson ImmunoResearch #001-000). After treatment, enteroids were fixed in 4% paraformaldehyde (Electron Microscopy Sciences #15710) for 10 minutes, then permeabilized with 0.2% Triton X-100 (Sigma-Aldrich #93443) for 10 minutes, and then washed. Samples were incubated overnight at 4°C with primary antibodies: Ki-67 (Santa Cruz #sc-7846); Villin (BD Transduction Labs #610358); Muc2 (Santa Cruz #sc-23170); Chromogranin A (Santa Cruz #sc-1488); DCLK-1 (Abcam #ab31704); GFP (Abcam #ab5450); Lysozyme (Agilent Technologies #A009902); Olfm4 (Santa Cruz #sc-84274); CD24 (BD Biosciences #553261); Actin, smooth Muscle Specific (Ab-2) (CalBioChem #CP47); pSMAD 1/5 (Cell Signaling #9516). Samples were then washed, stained with 1:1000-diluted secondary antibodies (AlexaFluor 488/546 αMouse/αRabbit, Life Technologies #A11008/A11003), and washed again. Secondary antibody alone was added to empty wells to serve as references for estimation of uneven illumination.

All non-antibody staining of enteroids was performed as a final step after antibody staining. DNA, actin, and Paneth cells were stained for 30 minutes with DAPI (Thermofisher #D21490), Hoechst (Invitrogen #H3570), Alexa Fluor 546 Phalloidin (Thermofisher #A12379), or UEA-1 Fluorescein (Vector labs #FL-1061), respectively. Click chemistry of EdU was also performed as a final step after prior antibody staining. Wells were incubated with 1 μM Alexa Fluor 488 Azide (Molecular Probes #A10266),1 mM CuSO4 (Sigma-Aldrich #451657), 500 mM L-Ascorbic acid (Sigma-Aldrich #A5960) in PBS for 30 minutes at room temperature. Wells were then washed 3 times in PBS and imaged. For

Annexin V staining, enteroids were washed with Annexin V binding buffer (AVBB; 10 mM HEPES pH 7.4, 150 mM NaCl, 2.5 mM CaCl2) and then incubated with 1:50 Cy5-conjugated Annexin V (BD Pharmigen #559934) at room temperature for 15 minutes. Enteroids were then washed with AVBB and immediately imaged.

Imaging—For imaging experiments, enteroid monolayers were plated in Falcon 96 Well, Black/Clear, Tissue Culture Treated Plates, Flat bottom with Lid (Cat# 353219). All plates were imaged using a GE® INCell 6000 automated microscope, 10X objective lens, and DAPI, FITC, and TRITC filter sets. All image analysis was performed using CellProfiler and custom Python scripts. Confocal microscopy was performed on a Zeiss LSM 780.

Quantification And Statistical Analysis

Image analysis and feature extraction—Cell nuclei in DAPI stain images were identified using two CellProfiler (Carpenter et al., 2006) pipelines that were specialized for identifying either densely packed (using the Propagate function in CellProfiler, which separates clumped objects using a voronoi-based method (Jones et al., 2005)) or sparsely packed (using the Shape function, which separates clumped objects using watershed on the distance-transform thresholded image (Wählby et al., 2004)) regions of nuclear staining. Custom Python scripts merged the two segmentations by identifying the dense and sparse regions: objects in the nuclear segmentation were dilated using a 5×5 kernel matrix, and resulting objects larger than 6000 pixels were defined as dense regions. Parameters for this algorithm were optimized using an expert-provided training set. Average nuclear intensity of EdU stains were extracted in CellProfiler. The EdU+ threshold was empirically set as >0.005 average nuclear EdU intensity. Paneth cells were segmented separately based on the UEA-1 (Paneth) stain images using the same nuclear segmentation pipeline. The CellProfiler pipelines were manually parameterized.

Crypt identification and measurement—To identify crypts, first dense regions were generated using the algorithm from above, with minimum area of 10,000 pixels. Then, dense regions containing at least 5 EdU positive cells were identified as crypt regions. Combining the crypt and cell segmentation, we measured crypt number and crypt size, which is the number of cells in the crypt. To measure dispersion of crypt regions, we measured the nearest neighbor distance of proliferative (EdU+) cells. For each EdU+ cell in a crypt, we calculated the distance to the nearest EdU+ cell in the same crypt. We can then construct a distribution of nearest EdU+ neighbor distances for each crypt that indicated the dispersion of crypt regions.

Statistical analysis—Data are presented as mean ± standard error of the mean (SEM) or mean ± standard deviation (SD), as indicated. Student's unpaired *t*-test was used to determine significant difference in quantification of control and perturbed cultures.

Data And Software Availability

Code samples will be posted to Github.

Supplementary Material

Refer to Web version on PubMed Central for supplementary material.

Acknowledgments

We are grateful to Sigurd B. Angenent, James J. Collins II, and Chonlarat Wichaidit for their insightful feedback. We thank David Manglesdorf, Ophir Klein, Frederic de Sauvage, and Genaro Hernandez for mouse resources and Andres Lorente-Rodriguez for the custom ImageJ macro. We also thank the anonymous reviewers for their helpful input. This work was supported by a Cancer Biology Training Grant T32 CA124334 (C.A.T.), an American Cancer Society–Lakeshore Division Postdoctoral Fellowship (C.A.T.), the National Institute of Health grants R00 DK103126 (C.A.T.), a National Science Foundation Graduate Research Fellowship (I.W.C), R37 DK34128 (M.H.C.), Welch I1243 (M.H.C.), GM112690 (S.J.A.) and R01CA184984 (L.F.W.), and the Institute of Computational Health Sciences (ICHS) at UCSF (S.J.A., L.F.W.).

References

Auclair BA, Benoit YD, Rivard N, Mishina Y, Perreault N. Bone morphogenetic protein signaling is essential for terminal differentiation of the intestinal secretory cell lineage. Gastroenterology. 2007; 133:887–896. [PubMed: 17678919]

Barker N, van Es JH, Kuipers J, Kujala P, van den Born M, Cozijnsen M, Haegebarth A, Korving J, Begthel H, Peters PJ, et al. Identification of stem cells in small intestine and colon by marker gene Lgr5. Nature. 2007; 449:1003–1007. [PubMed: 17934449]

Batts LE, Polk DB, Dubois RN, Kulessa H. Bmp signaling is required for intestinal growth and morphogenesis. Dev Dyn. 2006; 235:1563–1570. [PubMed: 16538672]

Boj SF, Hwang CI, Baker LA, Chio IIC, Engle DD, Corbo V, Jager M, Ponz-Sarvise M, Tiriac H, Spector MS, et al. Organoid models of human and mouse ductal pancreatic cancer. Cell. 2015; 160:324–338. [PubMed: 25557080]

Carpenter AE, Jones TR, Lamprecht MR, Clarke C, Kang IH, Friman O, Guertin DA, Chang JH, Lindquist RA, Moffat J, et al. CellProfiler: image analysis software for identifying and quantifying cell phenotypes. Genome Biol. 2006; 7:R100. [PubMed: 17076895]

Chen B, Dodge ME, Tang W, Lu J, Ma Z, Fan C-W, Wei S, Hao W, Kilgore J, Williams NS, et al. Small molecule-mediated disruption of Wnt-dependent signaling in tissue regeneration and cancer. Nat Chem Biol. 2009; 5:100–107. [PubMed: 19125156]

Cheng H, Leblond CP. Origin, differentiation and renewal of the four main epithelial cell types in the mouse small intestine V. Unitarian theory of the origin of the four epithelial cell types. Am J Anat. 1974; 141:537–561. [PubMed: 4440635]

Clevers HC, Bevins CL. Paneth cells: maestros of the small intestinal crypts. Annu Rev Physiol. 2013; 75:289–311. [PubMed: 23398152]

Crosnier C, Stamataki D, Lewis J. Organizing cell renewal in the intestine: stem cells, signals and combinatorial control. Nat Rev Genet. 2006; 7:349–359. [PubMed: 16619050]

Cuny GD, Yu PB, Laha JK, Xing X, Liu J-F, Lai CS, Deng DY, Sachidanandan C, Bloch KD, Peterson RT. Structure-activity relationship study of bone morphogenetic protein (BMP) signaling inhibitors. Bioorg Med Chem Lett. 2008; 18:4388–4392. [PubMed: 18621530]

Durand A, Donahue B, Peignon G, Letourneur F, Cagnard N, Slomianny C, Perret C, Shroyer NF, Romagnolo B. Functional intestinal stem cells after Paneth cell ablation induced by the loss of transcription factor Math1 (Atoh1). Proc Natl Acad Sci U S A. 2012; 109:8965–8970. [PubMed: 22586121]

van Es JH, Jay P, Gregorieff A, van Gijn ME, Jonkheer S, Hatzis P, Thiele A, van den Born M, Begthel H, Brabletz T, et al. Wnt signalling induces maturation of Paneth cells in intestinal crypts. Nat Cell Biol. 2005; 7:381–386. [PubMed: 15778706]

Ettayebi K, Crawford SE, Murakami K, Broughman JR, Karandikar U, Tenge VR, Neill FH, Blutt SE, Zeng XL, Qu L, et al. Replication of human noroviruses in stem cell-derived human enteroids. Science. 2016; 353:1387–1393. [PubMed: 27562956]

Farin HF, Van Es JH, Clevers H. Redundant sources of Wnt regulate intestinal stem cells and promote formation of Paneth cells. Gastroenterology. 2012; 143:1518–1529e7. [PubMed: 22922422]

Farin HF, Jordens I, Mosa MH, Basak O, Korving J, Tauriello DVF, de Punder K, Angers S, Peters PJ, Maurice MM, et al. Visualization of a short-range Wnt gradient in the intestinal stem-cell niche. Nature. 2016

Fevr T, Robine S, Louvard D, Huelsken J. Wnt/beta-catenin is essential for intestinal homeostasis and maintenance of intestinal stem cells. Mol Cell Biol. 2007; 27:7551–7559. [PubMed: 17785439]

Gao D, Vela I, Sboner A, Iaquinta PJ, Karthaus WR, Gopalan A, Dowling C, Wanjala JN, Undvall EA, Arora VK, et al. Organoid Cultures Derived from Patients with Advanced Prostate Cancer. Cell. 2014; 159:176–187. [PubMed: 25201530]

Haramis APG, Begthel H, van den Born M, van Es J, Jonkheer S, Offerhaus GJA, Clevers H. De novo crypt formation and juvenile polyposis on BMP inhibition in mouse intestine. Science. 2004; 303:1684–1686. [PubMed: 15017003]

He XC, Zhang J, Tong W-G, Tawfik O, Ross J, Scoville DH, Tian Q, Zeng X, He X, Wiedemann LM, et al. BMP signaling inhibits intestinal stem cell self-renewal through suppression of Wnt-beta-catenin signaling. Nat Genet. 2004; 36:1117–1121. [PubMed: 15378062]

Jones, TR., Carpenter, A., Golland, P. Computer Vision for Biomedical Image Applications. Springer; Berlin, Heidelberg: 2005. Voronoi-Based Segmentation of Cells on Image Manifolds; p. 535-543.

Lancaster MA, Renner M, Martin CA, Wenzel D, Bicknell LS, Hurles ME, Homfray T, Penninger JM, Jackson AP, Knoblich JA. Cerebral organoids model human brain development and microcephaly. Nature. 2013; 501:373–379. [PubMed: 23995685]

Maloy KJ, Powrie F. Intestinal homeostasis and its breakdown in inflammatory bowel disease. Nature. 2011; 474:298–306. [PubMed: 21677746]

McCracken KW, Catá EM, Crawford CM, Sinagoga KL, Schumacher M, Rockich BE, Tsai YH, Mayhew CN, Spence JR, Zavros Y, et al. Modelling human development and disease in pluripotent stem-cell-derived gastric organoids. Nature. 2014; 516:400. [PubMed: 25363776]

Moon C, VanDussen KL, Miyoshi H, Stappenbeck TS. Development of a primary mouse intestinal epithelial cell monolayer culture system to evaluate factors that modulate IgA transcytosis. Mucosal Immunol. 2014; 7:818–828. [PubMed: 24220295]

Ootani A, Li X, Sangiorgi E, Ho QT, Ueno H, Toda S, Sugihara H, Fujimoto K, Weissman IL, Capecchi MR, et al. Sustained in vitro intestinal epithelial culture within a Wnt-dependent stem cell niche. Nat Med. 2009; 15:701–706. [PubMed: 19398967]

Qi Z, Li Y, Zhao B, Xu C, Liu Y, Li H, Zhang B, Wang X, Yang X, Xie W, et al. BMP restricts stemness of intestinal Lgr5+ stem cells by directly suppressing their signature genes. Nat Commun. 2017; 8:13824. [PubMed: 28059064]

Radtke F, Clevers H. Self-renewal and cancer of the gut: two sides of a coin. Science. 2005; 307:1904–1909. [PubMed: 15790842]

San Roman AK, Jayewickreme CD, Murtaugh LC, Shivdasani RA. Wnt secretion from epithelial cells and subepithelial myofibroblasts is not required in the mouse intestinal stem cell niche in vivo. Stem Cell Reports. 2014; 2:127–134. [PubMed: 24527386]

Sato T, Vries RG, Snippert HJ, van de Wetering M, Barker N, Stange DE, van Es JH, Abo A, Kujala P, Peters PJ, et al. Single Lgr5 stem cells build crypt-villus structures in vitro without a mesenchymal niche. Nature. 2009; 459:262–265. [PubMed: 19329995]

Sato T, van Es JH, Snippert HJ, Stange DE, Vries RG, van den Born M, Barker N, Shroyer NF, van de Wetering M, Clevers H. Paneth cells constitute the niche for Lgr5 stem cells in intestinal crypts. Nature. 2010; 469:415. [PubMed: 21113151]

Sato T, Stange DE, Ferrante M, Vries RGJ, Van Es JH, Van den Brink S, Van Houdt WJ, Pronk A, Van Gorp J, Siersema PD, et al. Long-term expansion of epithelial organoids from human colon, adenoma, adenocarcinoma, and Barrett's epithelium. Gastroenterology. 2011; 141:1762–1772. [PubMed: 21889923]

Shyer AE, Huycke TR, Lee C, Mahadevan L, Tabin CJ. Bending gradients: how the intestinal stem cell gets its home. Cell. 2015; 161:569–580. [PubMed: 25865482]

Snippert HJ, van der Flier LG, Sato T, van Es JH, van den Born M, Kroon-Veenboer C, Barker N, Klein AM, van Rheenen J, Simons BD, et al. Intestinal crypt homeostasis results from neutral

competition between symmetrically dividing Lgr5 stem cells. Cell. 2010; 143:134–144. [PubMed: 20887898]

Terzić J, Grivennikov S, Karin E, Karin M. Inflammation and colon cancer. Gastroenterology. 2010; 138:2101–2114e5. [PubMed: 20420949]

Tian H, Biehs B, Warming S, Leong KG, Rangell L, Klein OD, de Sauvage FJ. A reserve stem cell population in small intestine renders Lgr5-positive cells dispensable. Nature. 2011; 478:255. [PubMed: 21927002]

VanDussen KL, Marinshaw JM, Shaikh N, Miyoshi H, Moon C, Tarr PI, Ciorba MA, Stappenbeck TS. Development of an enhanced human gastrointestinal epithelial culture system to facilitate patient-based assays. Gut. 2015; 64:911–920. [PubMed: 25007816]

Wählby C, Sintorn I-M, Erlandsson F, Borgefors G, Bengtsson E. Combining intensity, edge and shape information for 2D and 3D segmentation of cell nuclei in tissue sections. J Microsc. 2004; 215:67–76. [PubMed: 15230877]

Warmflash A, Sorre B, Etoc F, Siggia ED, Brivanlou AH. A method to recapitulate early embryonic spatial patterning in human embryonic stem cells. Nat Methods. 2014; 11:847–854. [PubMed: 24973948]

van de Wetering M, Francies HE, Francis JM, Bounova G, Iorio F, Pronk A, van Houdt W, van Gorp J, Taylor-Weiner A, Kester L, et al. Prospective derivation of a living organoid biobank of colorectal cancer patients. Cell. 2015; 161:933–945. [PubMed: 25957691]

Whitehead RH, Brown A, Bhathal PS. A method for the isolation and culture of human colonic crypts in collagen gels. In Vitro Cell Dev Biol. 1987; 23:436–442. [PubMed: 3597283]

Highlight

- Primary intestinal crypts form enteroid monolayers that recapitulate in vivo properties.
- Enteroid monolayers self organize from dissociated 3D organoids.
- Epithelium-intrinsic WNT and BMP signals can regulate intestinal tissue organization.
- Morphogenic signals establish tissue homeostasis through delayed feedback.

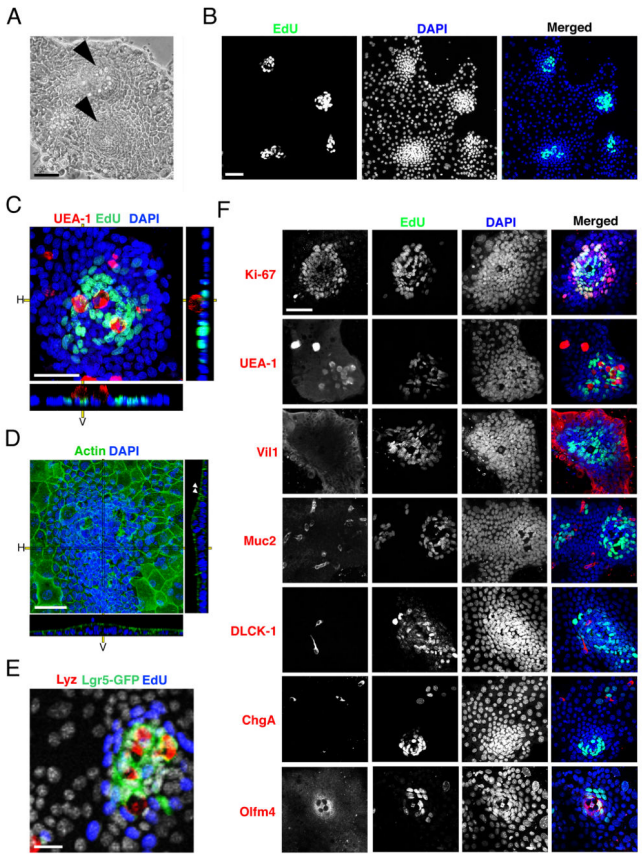

Figure 1.

Enteroid monolayers establish proliferative focal patterning and contain differentiated epithelial cell types. (**A**) Bright field images of 2D intestinal sheet 7 days after seeding. Arrowheads mark putative crypt foci. Scale bar = 25μM. (**B**) 2D intestinal cultures treated with EdU for 2 hours, then fixed and stained for EdU and DAPI. EdU clusters and dense nuclei foci co-localize (merged), indicating that the dense nuclear regions are proliferative crypt foci. Scale bar = 25μM. (**C**) Confocal image of crypt foci showing proliferative cells (EdU, green) clustered with Paneth cells (UEA-1, red) surrounded by non-proliferative cells (DAPI, blue). Scale bar = 25μM. (**D**) Confocal image of enteroid monolayers stained for actin (green) and DNA (blue). Arrowheads mark apical actin bundles. Right and bottom panels in c.–d. indicate horizontal (H) and vertical (V) projections. Scale bar = 25μM. (**E**) Enteroid monolayer cultures from $Lgr^{5eGFP\text{-}DTR}$ mice showing $Lgr5^{+}$ stem cells (green) juxtaposed with Paneth cells (lysozyme, red) and surrounded by proliferative TA cells (EdU, blue). Scale bar = 25μM. (**F**) Enteroid culture images co-stained for cell-fate marker (red: Ki-67 – proliferative; UEA-1 – Paneth; Muc2 – Goblet; villin – enterocyte; DCLK-1 – Tuft; ChgA – enteroendocrine; Olfm4 – stem), EdU (green) and DAPI (blue). Scale bar = 25μM. Crypts in B–F were seeded 7 days before staining and imaging. See also Figures S1, S2, and S3.

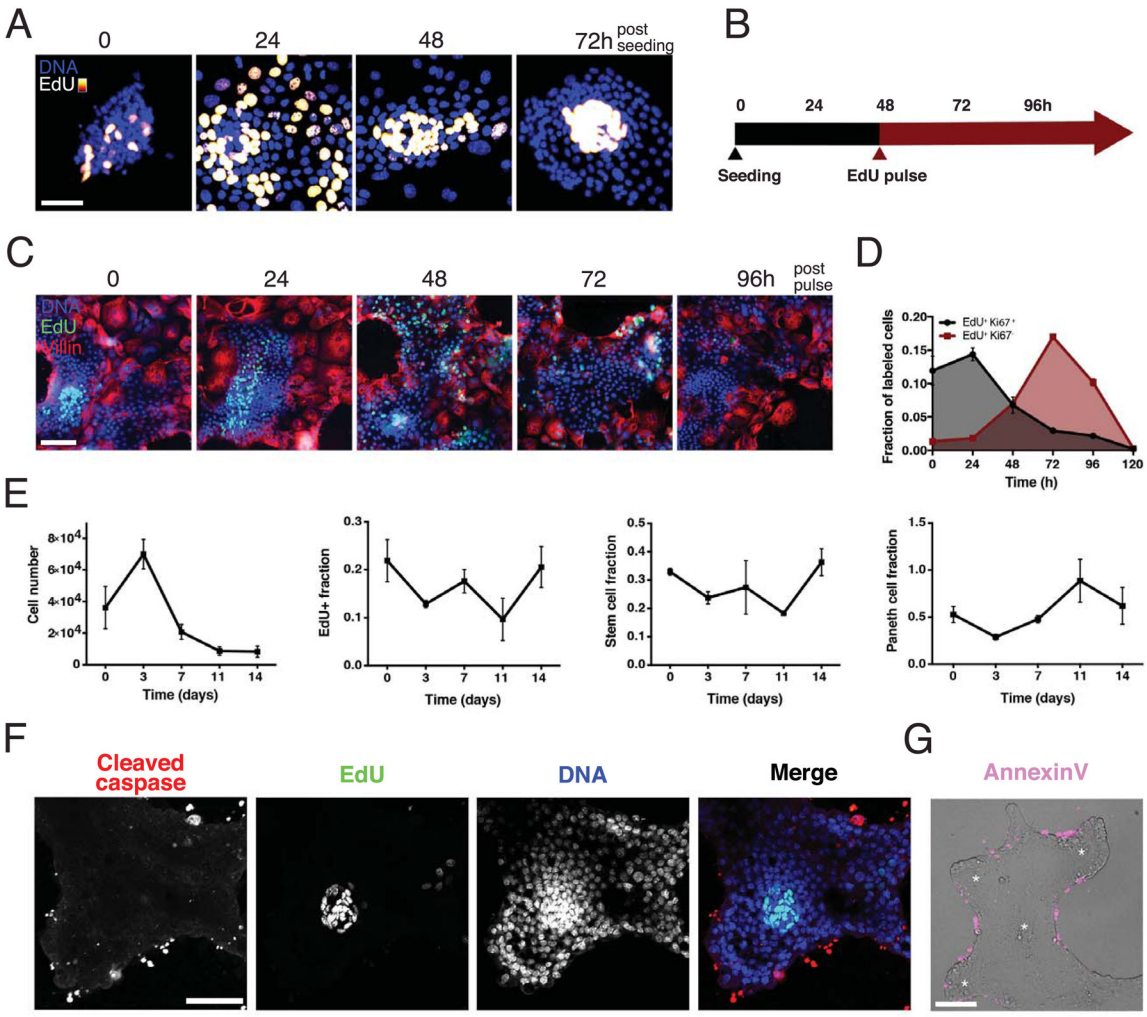

Figure 2.

Enteroid monolayers are dynamically established and maintained.

(**A**) Time course of crypt development after seeding on ECM. Cells labeled with EdU two hours before fixation at indicated time. Scale bar = 25 μM. (**B**) Timeline of experiments. **(C, D)**, Pulse-chase time-course experiment shows tissue turnover time of ~4 days. Enteroids were pulsed with EdU two hours prior to time 0 and then chased with fresh media lacking EdU. **(C)** Representative images of enteroid monolayer cultures, fixed and stained for DNA (blue), EdU (green) and Villin (red) at indicated times post EdU pulse. Scale bar = 50 μM. **(D)** Quantification of pulse-chase experiment showing colocalization of EdU with the proliferation marker Ki67 (grey, Ki-67^{+} and EdU^{+}) and colocalization of EdU with non-proliferative cells (red, Ki-67^{-} and EdU^{+}); Error bars represent mean ± SEM of triplicate wells, each containing ≥10000 cells. (**E**) Quantification of total cell number, fraction of EdU^{+}, fraction of stem cells (OLFM4^{+}), and fraction of Paneth cells (lysozyme^{+}) in enteroid cultures over a two-week time course. Error bars represent mean ± SEM of triplicate wells. (**F**) Cleaved caspase staining shows apoptosis occurs in the non-proliferative regions as opposed to the proliferative crypt regions (EdU+). Scale bar = 50 μM. (**G**) Annexin V

staining (magenta) overlay on phase contrast image shows cell death occurs on the margins of tissues. Asterisks denote clusters of Paneth cells. Scale bar = 50 μM. See also Figure S3.

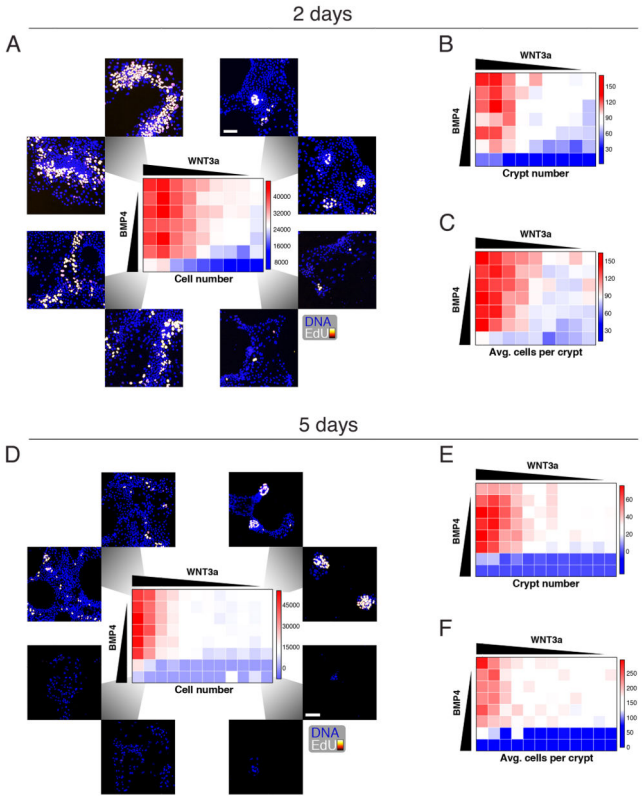

Figure 3.

The maintenance of growth and pattern formation for crypt foci is regulated by WNT and BMP. (**A**) Crypts were maintained for 2 days under a matrix of WNT3a vs. BMP4 concentrations in ENR media (see Experimental Procedures). Cells were labeled with EdU for two hours before fixation and staining for EdU and DNA. (**B,C**) As in (A), but crypt number (**B**) and average number of cells per crypt (**C**) were quantified. (**D**, **E**, **F**) As in (A–C) but with 5 days of growth factor treatment. Scale bars = 25 μM. See also Figure S3.

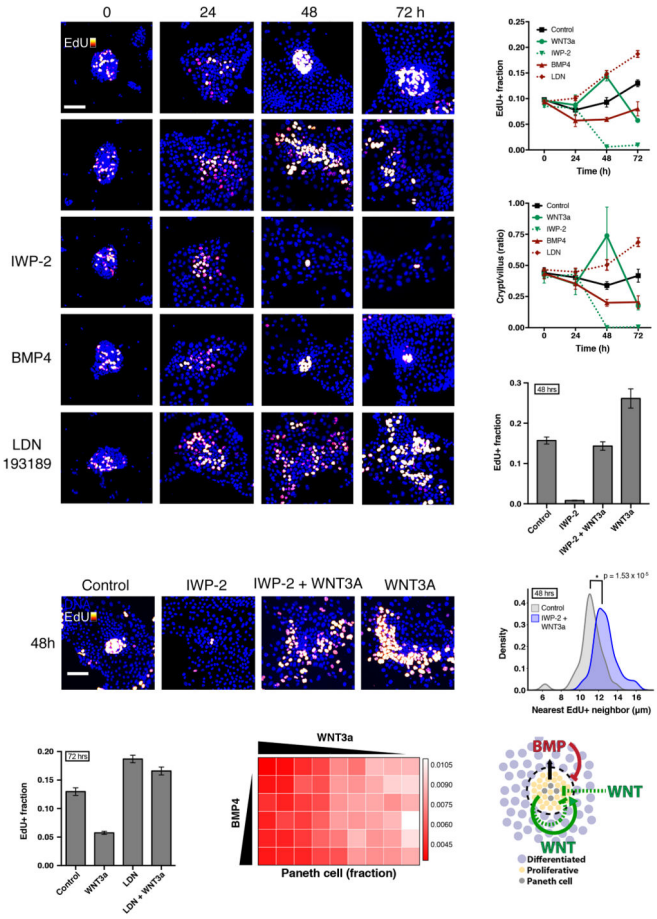

Figure 4.

The establishment of crypt foci requires intrinsic WNT and BMP signaling to regulate growth and patterning. (**A–F**) Enteroid monolayers respond to WNT or BMP after initial seeding. Four hours after seeding, cells were treated with ENR basal media and the indicated perturbation, WNT3a (8 nM), IWP-2 (10 uM), BMP4 (9 nM), or LDN (100 nM), throughout the time course. Cells were labeled with EdU two hours before fixation at the indicated time. (**A**) Staining of nuclei (DAPI) and proliferative cells (EdU). Scale bar = 50 μM. (**B,C**) Quantification of fraction EdU^+ cells (**B**), and ratio of crypt to villus cell numbers (**C**) of experiment in (A) throughout the time course. Error bars represent mean ± SEM of triplicate wells. (**D, E, F**) WNT3a treatment rescues proliferation but not patterning of enteroid monolayers. 48 hour treatment. (**D**) Quantification of fraction EdU^+ shows rescue of proliferation. Error bars represent mean ± SEM of triplicate wells. (**E**) Representative images of crypts under treatment at 48 hours. Scale bar = 50 μM. (**F**) Density plot of dispersion, as measured by distance between nearest neighbor EdU+ cells. Co-treatment with IWP-2 and WNT3a significantly shifts distribution compared to control. (**G**) Suppression of WNT3a-mediated growth collapse at 72 hours by LDN treatment. Error bars represent mean ± SEM of triplicate wells. (**H**) Quantification of fraction of Paneth cells out of total cells under 48 hours of WNT3a/BMP4 treatment. For morphogen concentrations,

see Experimental Procedures. (**I**) Model of tissue-autonomous growth and patterning self-regulation via WNT/BMP signaling. See also Figure S4.